NANO LETTERS

Letter

pubs.acs.org/NanoLett

Conformal Lithium Fluoride Protection Layer on Three-Dimensional Lithium by Nonhazardous Gaseous Reagent Freon

Dingchang Lin,[†] Yayuan Liu,[†] Wei Chen,[†] Guangmin Zhou,[†] Kai Liu,[†] Bruce Dunn,[‡] and Yi Cui*[,†,§]

[†]Department of Materials Science and Engineering, Stanford University, Stanford, California 94305, United States

[‡]Department of Materials Science and Engineering and California NanoSystems Institute, University of California, Los Angeles, Los Angeles, California 90095, United States

[§]Stanford Institute for Materials and Energy Sciences, SLAC National Accelerator Laboratory, 2575 Sand Hill Road, Menlo Park, California 94025, United States

Supporting Information

ABSTRACT: Research on lithium (Li) metal chemistry has been rapidly gaining momentum nowadays not only because of the appealing high theoretical capacity, but also its indispensable role in the next-generation Li−S and Li−air batteries. However, two root problems of Li metal, namely high reactivity and infinite relative volume change during cycling, bring about numerous other challenges that impede its practical applications. In the past, extensive studies have targeted these two root causes by either improving interfacial stability or constructing a stable host. However, efficient surface passivation on three-dimensional (3D) Li is still absent. Here, we develop a conformal LiF coating technique on Li surface with commercial Freon R134a as the reagent. In contrast to solid/liquid reagents, gaseous Freon exhibits not only nontoxicity and well-controlled reactivity, but also much better permeability that enables a uniform LiF coating even on 3D Li. By applying a LiF coating onto 3D layered Li-reduced graphene oxide (Li-rGO) electrodes, highly reduced side reactions and enhanced cycling stability without overpotential augment for over 200 cycles were proven in symmetric cells. Furthermore, Li−S cells with LiF protected Li-rGO exhibit significantly improved cyclability and Coulombic efficiency, while excellent rate capability (~800 mAh g^{-1} at 2 C) can still be retained.

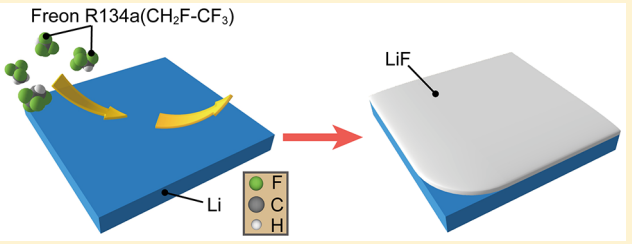

KEYWORDS: *Lithium metal anodes, three-dimensional Li, stable host, interface passivation, artificial SEI*

The advent of lithium (Li)-ion batteries, which exhibit unrivaled energy density among commercial battery chemistries, has been a grand success in extensively revolutionizing the fields of portable electronics, electric vehicles, and showing great potential for stationary energy storage.[1−3] However, after three decades of development, conventional Li-ion batteries have approached their limits and encountered challenges to catch up with the growing demands of higher energy density and power-intensive applications.[1,3] Li metal anodes hold great promises that go beyond Li-ion chemistries, where their high specific capacity (3860 mAh g^{-1}) and lowest electrochemical potential (−3.04 V versus standard hydrogen electrode) guarantee their role as the ultimate chemistry for high-energy Li battery systems.[4,5] Furthermore, as one of the key components in the prominent Li−S and Li−air battery systems,[6] developing Li metal anodes becomes a prerequisite for their successful commercialization in the future.

In fact, at the infant stage of Li batteries, Li metal was considered preferentially as the choice for anodes.[7,8] However, after nearly five decades of research, its implementation is still stagnant due to the severe safety hazards and poor electrochemical stability, which originate from the interfacial fluctuation, unstable solid−electrolyte interphase (SEI), and dendrite deposition.[4,5,9−11] In the past, various approaches such as engineering high-modulus solid electrolyte,[12−14] developing electrolyte additives,[15−17] and application of surface passivation[18] have been examined, which partially solved the problems yet far from satisfactorily. Recently, the introduction of nanotechnologies facilitates the renaissance of Li metal and reignites the hope of solving the overall problems.[4] Engineering interfaces,[19−22] homogenizing ion flux,[23−26] and designing stable "host"[27−31] have shown great promise in addressing the multifaceted issues. It is noted that whatever strategies are considered, the Li surface protection is a perennial subject of interest due to the spontaneous side reactions between highly reactive Li metal and liquid electrolytes. Without an adequate surface protection, the parasitic reactions would occur and result in thick and nonuniform SEI, which could further contribute to other issues including SEI fracture, dendritic Li deposition, and low Coulombic efficiency (CE).

Received: March 9, 2017
Revised: May 15, 2017
Published: May 23, 2017

DOI: 10.1021/acs.nanolett.7b01020
Nano Lett. XXXX, XXX, XXX−XXX

Among the surface protection materials, Li fluoride (LiF) has gained special attention due to its wide electrochemical stability window with negligible solubility in most of the electrolytes as well as its capability of regulating surface tension.[32,33] In the early stage, it was found that the addition of HF or fluorinated compounds into electrolyte would help form LiF in SEI and enable more uniform Li deposition.[34,35] Later, utilizing LiF additive in electrolyte was also proven efficacious to stabilize the SEI and homogenize Li plating.[36] However, these methods are unlikely to produce high-quality continuous and conformal LiF coating on Li metal. Instead, dispersive LiF domains would form with many weakly linked grain boundaries, which would easily fracture during Li metal plating and stripping. Moreover, HF and other fluorinated compounds are highly hazardous reagents, which might impose extra challenges in either industrial processing or battery packaging.

In addition, the infinite relative volume change of planar Li foil adopted previously brings about grand challenges to the protection layer. The inorganic protection layers can hardly accommodate the huge interface fluctuation of tens of micrometers.[4,27,31] As a consequence, a 3D form of Li with stable host will be a much better platform for surface protection.

Herein, we developed a conformal LiF surface coating strategy enabled by the reaction between nonhazardous gaseous Freon R134a (1,1,1,2-tetrafluoroethane) and Li metal. Noticeably, the gas-phase reagent is a desirable choice that provides high accessibility of precursors to Li surface and much improved film homogeneity. By exposing Li metal to Freon R134a gas, assisted with controlled gas pressure, and reaction temperature, we were able to coat a dense and uniform LiF layer with tunable thickness directly onto metallic Li. The above merits together offer the exciting opportunity to obtain conformal surface protection on the 3D form of Li, which has not been well achieved before. After application of the conformal LiF coating on layered Li-reduced graphene oxide (Li-rGO) composites, we realized further improved interfacial stability in addition to highly reduced relative volume fluctuation, which was demonstrated by electrochemical impedance spectroscopy (EIS) study prior to cell operation. Symmetric-cell cycling corroborated the enhanced stability with LiF coating in prolonged cycles, during which neither voltage fluctuation nor increase could be observed. Moreover, Li−S prototype cells with LiF-coated layered Li-rGO as the anode were examined, which exhibited further improved cycling stability and CE and confirmed good surface passivation and thus reduced shuttle effect. By realizing high-quality LiF coating on any forms of Li surface, this work demonstrates the great feasibility as well as the advantages of gas-phase reactions for Li surface protection, and it paves the way for the stable and safe operation of Li metal anode in the future. The as-developed methodology can also inspire further efforts on Li surface modification by other inorganic/organic compounds with similar gaseous reagents.

Figure 1a schematically shows the major LiF coating procedures using gaseous Freon R134a as the reagent. When Li is exposed to Freon R134a gas in a hermetic vessel, Freon R134a would spontaneously react with Li and form a layer of LiF on the surface. The hermetic vessel used in this experiment is shown in Figure S1, where a pressure gauge was designed to control the gas pressure in the vessel, while a flat pedestal enabled the heating of the vessel at the bottom. Started with a vacuumed vessel where Li was adhered inside at the bottom, a certain amount of Freon R134a gas was filled in, which was determined by the reading on the pressure gauge. Afterward, the vessel was heated on a hot plate with calibrated surface temperature. By tuning the gas pressure and reaction temperature, we were able to search the optimized parameters for the formation of high-quality LiF coating. The chemical reaction at the early stage is proposed in Figure 1b, where a C−F bond was first broken by metallic Li as a strong electron donor to form LiF, followed by the electron transfer from another Li atom to the central carbon. The formation of $(CH_2F\text{-}CF_2)^-Li^+$ would be preferential since the high electronegativity of the two F atoms would help stabilize negatively charged central carbon. Afterward, either α or β elimination could occur to further obtain LiF, forming either a carbene or an olefin, respectively. Further reactions can be much more complex with numerous possible products, during which the other F atoms can further react to yield more LiF.

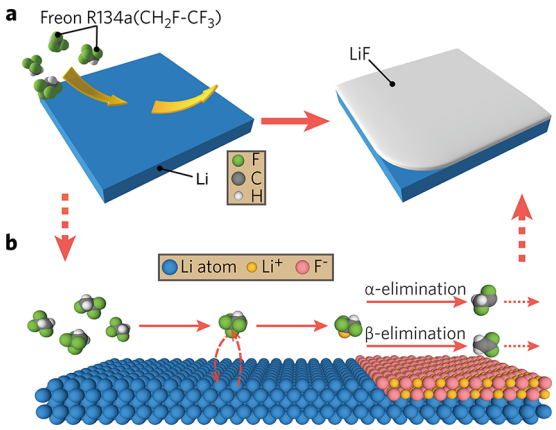

Figure 1. Schematic diagrams of surface LiF coating and major chemical reactions at the early stage. (a) Schematic showing the surface treatment of Li metal with Freon R134a, which helps form a conformal LiF coating on the Li metal surface. (b) Proposed major chemical reactions at the early stage of surface treatment, where $(CH_2F\text{-}CF_2)^-Li^+$ can form as an intermediate followed by either α or β elimination. LiF is the products of the reactions. The further reactions can be rather complex with numerous possibilities of products.

To optimize the parameters for high-quality LiF coating, gas pressure and reaction temperature were tuned accordingly, with the surface and cross-section morphologies under different conditions shown in Figures S2 and S3, respectively. It was found that at a fixed temperature, increasing gas pressure would accelerate the reaction and afford rougher surface. When gas pressure was fixed, the reactivity increased with temperature as well. At temperature below 150 °C, the surface was smooth without visible domains, while the reaction rate dropped with decreasing temperature. However, once the temperature was increased to ∼180 °C, approaching the melting point of Li metal, the reaction occurred in a much more vigorous fashion and formed micron-sized and porous LiF domains. Thus, to obtain high-quality LiF coating and sufficient reaction rate, 150 °C and 0.5 atm is a good condition for conducting the surface coating. The low magnification SEM images were also shown in Figure S4, which proves the good uniformity of the LiF film in large area. With the high quality LiF passivation layer, we have further proven highly improved ambient stability (Figure S5).

Figure 2a and b show the top surface and cross section of LiF-coated Li foil obtained at 150 °C and 0.5 atm for 20 h, respectively. It is noted that even at high magnification, the

DOI: 10.1021/acs.nanolett.7b01020
Nano Lett. XXXX, XXX, XXX−XXX

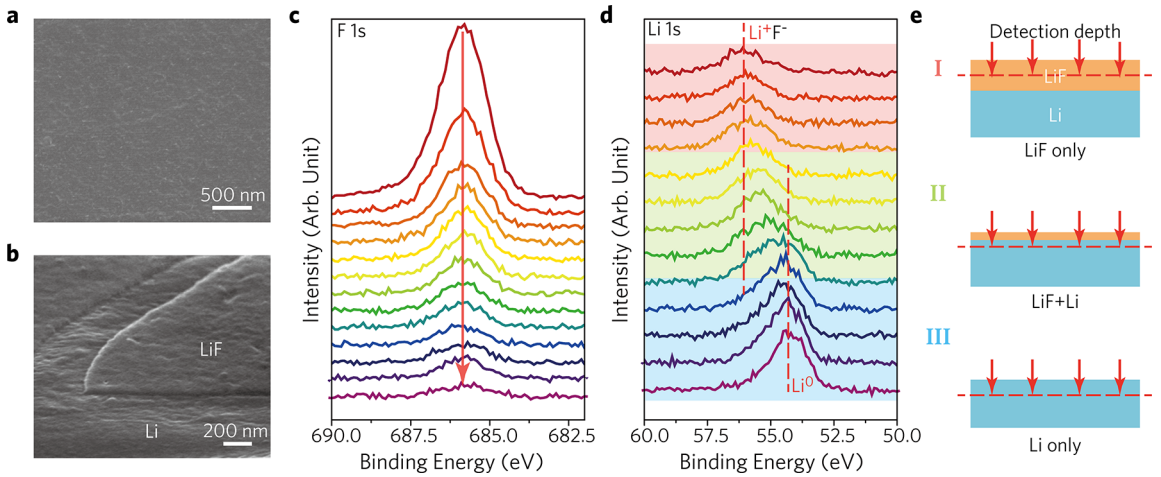

Figure 2. Characterizations of the LiF coating on Li foils. (a, b) High-resolution SEM images showing the (a) surface morphology and (b) cross-section of a LiF-coated Li foil. The top view shows smooth LiF surface, and the cross-section image indicates its uniform thickness of ~40 nm. (c, d) XPS depth profiles of (c) F 1s and (d) Li 1s. Starting from the curve on the top, 30 s sputtering was performed between two measurements. Gradual decrease of F 1s signal was observed after sputtering, which indicated reduced amount of LiF. In contrast, Li^+ signal in LiF was observed at the early stages without Li^0 signal, followed by the coexistence of the both signals at the intermediate stages. At the end, only Li^0 was shown. The stages in region I (red), II (green) and III (blue) were schematically shown in panel e, where the detection depth of XPS covers only LiF layer, LiF+Li, and only Li, respectively.

surface still exhibits dense and smooth morphology, without observable pinholes or grain boundaries. Twenty hours of reaction at this condition afforded LiF with thickness of ~40 nm. The X-ray photoelectron spectroscopy (XPS) depth profiles further demonstrated the dense and uniform nature of the as-formed LiF film (Figure 2c,d; Figure S6). As shown in Figure 2c, after multiple sputtering, the signal of F 1s dropped gradually, which indicated the reduced thickness of LiF layer. Accordingly, The Li 1s signal was fixed at ~56.2 eV at the early stages (red region, I), corresponding to the Li-ion in LiF (Figure 2d), followed by gradual shift to lower binding energy (green region, II). At the final stages (blue region, III), the major peak of Li 1s was at ~54.2 eV, which originated from the metallic Li foil underneath the original LiF film. Figure 2e schematically shows the different stages in the depth profile analysis. At the early stage (red region, I), since the LiF was thick and dense, metallic Li underneath the LiF film could not be detected. Once the LiF film was gradually removed, the metallic Li underneath fell into the detection region and its signal started to emerge, showing as the gradually shift of Li 1s to lower binding energy in green region (II). Finally, when LiF was almost vanished, only the peak of Li metal was left. In addition, the depth profile of C 1s XPS signal (Figure S7) shows the existence of CF and CF_2 groups, which is consistent with the products of proposed reactions. The as-grown LiF film on the Li foil was further confirmed to be crystalline phase, where the characteristic peaks were observed in X-ray diffraction (Figure S8).

Constructing a stable scaffold for Li metal has been proven to be of great importance due to its highly reduced volume variation and thus more stable SEI formation. The resulting enhanced active surface area would also homogenize the ion flux and enable more uniform Li deposition. However, the increase in active surface, if exposed directly to the electrolyte, can also lead to more SEI formation at the early stage, which is undesirable in view of reducing side reaction. As a consequence, it is beneficial to protect the interface beforehand with the as-developed conformal LiF coating. Here, the LiF protection coating was applied onto layered Li-rGO composite electrodes (Figure S9). The cross-section SEM images (Figure 3a) show the layered Li-rGO before (top) and after (bottom) LiF coating, where a conformal surface layer was observed after the coating was applied. This LiF coating would not only efficiently passivate the reactive surfaces, reducing the initial side reaction, but also enable more uniform composition of SEI.

To study the efficacy of the LiF coating for improving electrochemical stability, symmetric cells were first assembled and tested. Without further notice, 1 M $LiPF_6$ in 1:1 v/v ethylene carbonate (EC)/diethyl carbonate (DEC) was used as the standard electrolyte. Figure 3b shows the time-dependent electrochemical impedance spectroscopy (EIS) studies of the layered Li-rGO electrodes at the open circuit condition prior to electrochemical cycling. Without LiF coating (Figure S10), the layered Li-rGO electrodes exhibit gradually increased resistance within the first 12 h, which is the result of the accumulation of SEI at the early stage. In contrast, the LiF-coated counterparts do not show obvious increase in impedance within the same period of time (Figure 3b), indicating robust surface passivation that suppressed continuous side reactions and reduced the initial SEI formation. To determine the effect of LiF coating on the kinetics of the electrode, exchange current was measured with a three-electrode cell (Figure S11). A slightly reduced exchange current density was observed for LiF coating on Li-rGO, from ~0.95 mA cm^{-2} to ~0.69 mA cm^{-2} (Figure 3c), which is still much higher than that of planar Li foil (~0.041 mA cm^{-2}, Figure S12a). For planar Li foil, the low exchange current density indicates its rather sluggish kinetics even without LiF coating. A LiF coating on this planar Li further exacerbated the situation, reaching a low exchange current density of ~0.012 mA cm^{-2} (Figure S12b). The stark differences manifest the necessity to develop 3D form of Li with passivation LiF coating. On the basis of the exchange current measurement, the ionic conductivity of the LiF layer was further estimated to be ~3×10^{-9} S cm^{-1} (detail of calculation was included in the Supporting Information), similar to the value reported elsewhere.[37] The further cycling stability of symmetric cells is compared in Figure 3d, where the current density and plating/stripping capacity were fixed at 1

DOI: 10.1021/acs.nanolett.7b01020
Nano Lett. XXXX, XXX, XXX−XXX

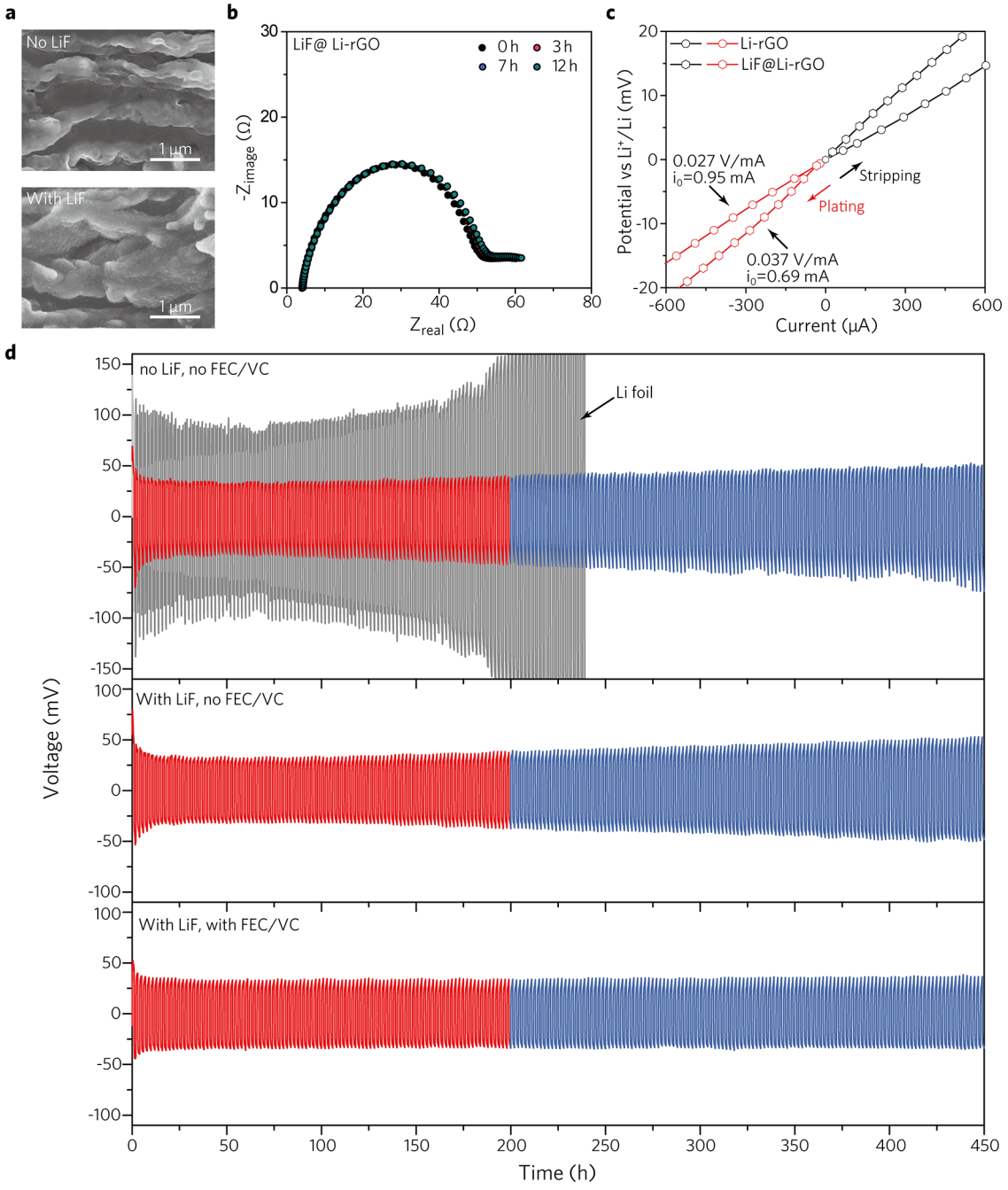

Figure 3. Electrochemical characterizations of LiF-coated layered Li-rGO electrodes. (a) Cross-section SEM images of layered Li-rGO before (top) and after (bottom) LiF coating, where a conformal surface layer can be observed after coating. The observed edge was obtained before LiF coating. (b) Time-dependent Nyquist plots of electrochemical impedance measurement on symmetric cells with LiF coating. The cells with LiF@Li-rGO did not show obvious increase in resistance, which is due to the good surface passivation that reduces the side reactions. (c) Linear sweep voltammetry measurement showing the exchange current density with (hexagon) and without (circle) LiF coating. (d) Symmetric-cell cycling of the layered Li-rGO cells without LiF and FEC/VC additives (top), with LiF but without FEC/VC additives (middle), and with both LiF and FEC/VC additives (bottom). The red curves represent the first 100 cycles, while the blue parts show the post-100 cycles. The cycling stability of the layered Li-rGO symmetric cells increases from the top to bottom. The gray curve in the top figure shows the cycling stability of a Li foil symmetric cell in the electrolyte without FEC/VC additives.

mA cm^{-2} and 1 mAh cm^{-2}, respectively. In the figure, red curves represent the first 100 cycles, while the post-100 cycles are plotted in blue. It is noted that for the layered Li-rGO cells without LiF (top), the cycling stability already outperforms that of Li foil cells (gray curve, top), with consistently lower polarization as well as flat voltage plateaus. However, slightly increased overpotential can still be observed after 100 cycles, which illustrates the existence of side reaction to some extent in prolonged cycles. After the LiF coating (middle) was applied, improved cycling stability especially in the later cycles could be observed. Nevertheless, the polarization still exhibits minor increases, which can be attributed to the fragile nature of inorganic LiF films, where cracks might form in the extended cycles. This effect can be resolved by the addition of

DOI: 10.1021/acs.nanolett.7b01020
Nano Lett. XXXX, XXX, XXX−XXX

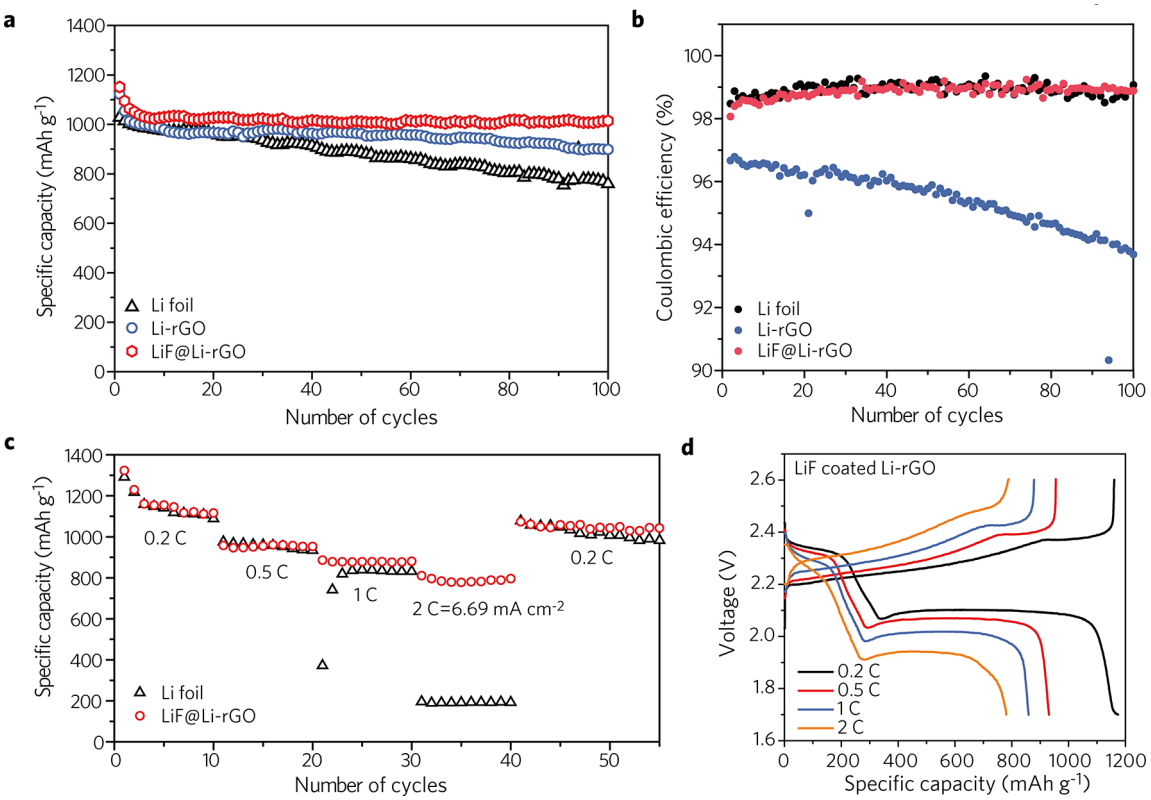

Figure 4. Electrochemical characterizations of Li−S prototype cells. (a) Comparison on cycling stability of Li−S prototype cells with Li foil, Li-rGO, and LiF-coated Li-rGO as the anodes. (b) Corresponding Coulombic efficiency. (c) Rate capability of the Li−S cells with Li foil and LiF-coated Li-rGO as the anodes. (d) Corresponding voltage profiles of a Li−S cell with LiF coated Li-rGO as the anode at various rates from 0.2 to 2 C. The areal mass loading of S is 2.0 mg cm^{-2}. The rate is calculated based on the theoretical capacity of S, where 2 C is equivalent to 6.69 mA cm^{-2}.

fluoroethylene carbonate (FEC, 10%) and vinylene carbonate (VC, 1%) in the electrolyte. On one hand, FEC can be reduced by exposed Li once the cracks form, with the formation of new LiF that can instantly heal the cracks. On the other hand, the existence of VC in the electrolyte can polymerize on the anode surface, stabilizing the SEI by improving its flexibility. As a consequence, much more stable cycling can be achieved by the synergy of conformal LiF coating and the electrolyte additives, without observable augment in overpotential even after 200 cycles.

The protection effect of the LiF coating on layered Li-rGO electrodes was further examined in the Li−S prototype cells, which are widely recognized as a promising candidate for the next-generation energy storage. However, its poor cyclability, unstable Li anode, and polysulfide shuttle effect prevent it from becoming a viable technology.[6,38,39] Although constructing a stable host for Li can extend the cycle life and stabilize the anode, the increased surface area of Li brings about severe Li polysulfide shuttle effect and thus low CE. Figure 4a shows the cycling of Li−S cells at a constant charge/discharge rate of 0.5 C, where the layered Li-rGO electrodes consistently exhibited much better cycling stability compared with the Li foil cell. However, the layered Li-rGO cell without LiF coating afforded lower CE than the Li foil cell (Figure 4b), which can be attributed to the highly increased exposed Li surface that exacerbates the shuttling of Li polysulfide species. The dilemma can be well addressed by the conformal LiF coating on the layered Li-rGO electrodes. As shown in Figure 4a and b, a conformal LiF coating on layered Li-rGO can further stabilize the cycling, with high capacity retention above 1000 mAh g^{-1} for at least 100 cycles. More importantly, the LiF protection layer can also simultaneously passivate the surface and improve the average CE significantly from ~95% (blue) to ~99% (red). It is also noted that more stable voltage profiles can be obtained for the LiF coated Li-rGO cells (Figure S14), which further support the efficient surface passivation and thus more stable SEI. Moreover, the LiF coated Li-rGO cells also exhibit highly improved rate capability compared with the Li foil counterparts especially at high rates. It is shown in Figure 4c that the LiF coated Li-rGO cells retain a high capacity of ~800 mAh g^{-1} even at a high rate of 2 C, equivalent to a current density of 6.69 mA cm^{-2}. The voltage profiles at different rates are further shown in Figure 4d, where low overpotential can be consistently observed at various rates. In contrast, the capacity of Li foil cells drops to less than 200 mAh g^{-1} at the same rate, losing its second plateau in the voltage window of 1.7−2.6 V (Figure S15). The improved rate capability can be attributed to the reduced polarization at the anode side by the increased active surface and the homogenized ion flux.

In all, a facile and controllable method for generating conformal LiF coating on Li was for the first time fulfilled with gaseous Freon R134a as the reagent. The gaseous Freon R134a guaranteed not only controllable reactivity, nontoxicity, and industrial accessibility, but also better permeability than solid/liquid precursors and thus more uniform LiF coating on planar and even 3D forms of Li. Specifically, after the conformal LiF coating was applied onto layered Li-rGO electrodes, highly improved interfacial stability and reduced side reactions were fulfilled. As a result, the symmetric-cell cycling demonstrates further improved stability, without observable overpotential

DOI: 10.1021/acs.nanolett.7b01020
Nano Lett. XXXX, XXX, XXX−XXX

augment even for over 200 cycles. Moreover, Li−S prototype cells were demonstrated with the LiF protected Li-rGO electrodes, where much enhanced cyclability and CE were observed as a result of good surface passivation. At the same time, the Li−S cells with LiF coated Li-rGO still retain high rate capability (~800 mAh g^{-1} at 2 C), outperforming its Li foil counterpart especially at the high rate of 2 C. We believe that the as-developed conformal LiF coating method would enlighten more strategies on Li surface protection and offer exciting opportunities for high-energy battery systems with stable Li metal anode.

Methods. *Conformal LiF Coating on Li Metal with Freon 134a.* To conduct the reaction between Freon R134a and Li metal, a hermitic vessel was designed and assembled as shown in Figure S1. Before reactions, Li electrodes were adhered to the stainless steel KF40 blank flange in a glovebox with subppm of O_2 level, followed by the sealing of the vessel with a clamp. Afterward, the vessel was vacuumed by exhausting the gas through the valve on the top. Once the vessel was vacuumed, a certain amount of Freon R134a gas was filled in through the top valve and sealed. The Freon amount was controlled by the reading on the pressure gauge. Then the vessel was heated on a hot plate, while the surface temperature of the hot plate was calibrated by a surface temperature thermometer. Finally, the vessel was dissembled to obtain the LiF coated Li electrodes when the reaction was complete.

Materials Characterizations. The SEM images were taken with a FEI XL30 Sirion scanning electron microscope. ImageJ was used to measure the thickness of LiF. XPS anyalysis was obatained on a PHI VersaProbe 1 scanning XPS microprobe with Al (Kα) source. The XPS depth profiles were obtained by interval sputtering time of 30 s between two acquirement. The sputtering process helps remove the material layer-by-layer on the characterized surface. The sputtering rate calibrated by SiO_2 was ~12 nm min^{-1}. X-ray diffraction was measured on a Bruker D8 Venture with Cu (Kα) source.

Electrochemical Tests on the Symmetric Cells. The 2032-type coin cells (MTI) were used to assembled the cells. The symmetric cells consisted of the same electrode at the both sides. Layered Li-rGO (~16 mAh cm^{-2}) with and without LiF coating and Li foils (750 μm, 99.9%, Alfa Aesar) were used for comparison. Without further notice, the electrolyte employed was 1 M lithium hexafluorophosphate ($LiPF_6$) in 1:1 ethylene carbonate (EC)/diethyl carbonate (DEC) (BASF Selectilyte LP40) without other additives. For the tests with additives in the electrolyte, 10% fluoroethylene carbonate (FEC, Novolyte Technologies Inc.) and 1% vinylene carbonate (VC, Novolyte Technologies Inc.) were added into the above blank electrolyte. Celgard 2325 (25 μm PP/PE/PP) was used as the separator. Galvanostatic cycling was conducted on a LAND 8-channel battery tester. The electrochemical impedance spectroscopy was measured on a Biologic VMP3 system.

Lithium Polysulfide (Li_2S_8) Catholyte Preparation. To prepare 5 M Li_2S_8 solution, 0.56 g of sulfur and 0.115 g of Li_2S were added sequentially into 4 mL of 1:1 v/v DOL/DME solution. No lithium nitrate was added to the catholyte solution. The obtained suspension was stirred and heated at 80 °C overnight to yield red−brown Li_2S_8 solution.

Li−S Batteries Tests. The 2032-type coin cells (MTI) were assembled to examine the Li−S prototype cells. Pyrograf-III carbon nanofiber was filtrated to form a film as the cathode current collector. The above-synthesized 5 M Li_2S_8 (2 mg equivalent mass loading of sulfur), 12.5 μL, was uniformly dropcast onto a carbon nanofiber film as the cathode. The electrolyte was freshly prepared by dissolving 1 M LiTFSI in 1:1 v/v DOL/DME containing $LiNO_3$ (1 wt %). Electrolyte in each cell was fixed to be 20 μL. Celgard 2325 (25 μm PP/PE/PP) was used as the separator. The rate capability test of the cells was carried out using a LAND 8-channel battery tester.

■ ASSOCIATED CONTENT

Supporting Information

The Supporting Information is available free of charge on the ACS Publications website at DOI: 10.1021/acs.nanolett.7b01020.

Supplementary methods, experimental setups, additional SEM, XPS, XRD characterizations, air stability tests, and additional electrochemical tests (PDF)

■ AUTHOR INFORMATION

Corresponding Author

*E-mail: yicui@stanford.edu.

ORCID

Dingchang Lin: 0000-0002-9354-5952
Wei Chen: 0000-0001-7701-1363
Kai Liu: 0000-0003-3362-180X
Bruce Dunn: 0000-0001-5669-4740

Author Contributions

D.L., B.D. and Y.C. conceived the concept and designed the experiments. D.L. designed the hermitic vessel. W.C. helped with the assembly of the vessel. D.L. performed the LiF coating experiments D.L. conducted most of the characterizations and the electrochemical measurement. Y.L. and K.L. helped with materials characterizations. D.L. and G.Z. performed the Li−S batteries. D.L. and Y.C. cowrote the paper. All authors discussed the results and commented on the manuscript.

Notes

The authors declare no competing financial interest.

■ ACKNOWLEDGMENTS

We thank Dr. Arturas Vailionis for assistance in XRD measurements and Junzhe Lou for helpful discussion on chemical reaction mechanisms. Y.C. acknowledges the support from the Assistant Secretary for Energy Efficiency and Renewable Energy, Office of Vehicle Technologies of the U.S. Department of Energy under the Battery Materials Research (BMR) program and Battery500 consortium.

■ REFERENCES

(1) Tarascon, J.-M.; Armand, M. *Nature* **2001**, *414* (6861), 359−367.
(2) Dunn, B.; Kamath, H.; Tarascon, J.-M. *Science* **2011**, *334* (6058), 928−935.
(3) Goodenough, J. B.; Park, K.-S. *J. Am. Chem. Soc.* **2013**, *135* (4), 1167−1176.
(4) Lin, D.; Liu, Y.; Cui, Y. *Nat. Nanotechnol.* **2017**, *12* (3), 194−206.
(5) Xu, W.; Wang, J.; Ding, F.; Chen, X.; Nasybulin, E.; Zhang, Y.; Zhang, J.-G. *Energy Environ. Sci.* **2014**, *7* (2), 513−537.
(6) Bruce, P. G.; Freunberger, S. A.; Hardwick, L. J.; Tarascon, J.-M. *Nat. Mater.* **2011**, *11* (1), 19−29.
(7) Brandt, K. *Solid State Ionics* **1994**, *69* (3−4), 173−183.
(8) Whittingham, M. S. *Chem. Rev.* **2004**, *104* (10), 4271−4302.
(9) Aurbach, D. *J. Power Sources* **2000**, *89* (2), 206−218.
(10) Xu, K. *Chem. Rev.* **2004**, *104* (10), 4303−4418.
(11) Xu, K. *Chem. Rev.* **2014**, *114* (23), 11503−11618.

DOI: 10.1021/acs.nanolett.7b01020
Nano Lett. XXXX, XXX, XXX−XXX

(12) Bouchet, R.; Maria, S.; Meziane, R.; Aboulaich, A.; Lienafa, L.; Bonnet, J.-P.; Phan, T. N.; Bertin, D.; Gigmes, D.; Devaux, D.; et al. *Nat. Mater.* **2013**, *12* (5), 452−457.
(13) Lin, D.; Liu, W.; Liu, Y.; Lee, H. R.; Hsu, P.-C.; Liu, K.; Cui, Y. *Nano Lett.* **2016**, *16* (1), 459−465.
(14) Stone, G.; Mullin, S.; Teran, A.; Hallinan, D.; Minor, A.; Hexemer, A.; Balsara, N. *J. Electrochem. Soc.* **2012**, *159* (3), A222−A227.
(15) Ding, F.; Xu, W.; Graff, G. L.; Zhang, J.; Sushko, M. L.; Chen, X.; Shao, Y.; Engelhard, M. H.; Nie, Z.; Xiao, J.; et al. *J. Am. Chem. Soc.* **2013**, *135* (11), 4450−4456.
(16) Li, W.; Yao, H.; Yan, K.; Zheng, G.; Liang, Z.; Chiang, Y.-M.; Cui, Y. *Nat. Commun.* **2015**, *6*, 7436.
(17) Qian, J.; Henderson, W. A.; Xu, W.; Bhattacharya, P.; Engelhard, M.; Borodin, O.; Zhang, J.-G. *Nat. Commun.* **2015**, *6*, 6362.
(18) Kozen, A. C.; Lin, C.-F.; Pearse, A. J.; Schroeder, M. A.; Han, X.; Hu, L.; Lee, S.-B.; Rubloff, G. W.; Noked, M. *ACS Nano* **2015**, *9* (6), 5884−5892.
(19) Zheng, G.; Lee, S. W.; Liang, Z.; Lee, H.-W.; Yan, K.; Yao, H.; Wang, H.; Li, W.; Chu, S.; Cui, Y. *Nat. Nanotechnol.* **2014**, *9* (8), 618−623.
(20) Yan, K.; Lee, H.-W.; Gao, T.; Zheng, G.; Yao, H.; Wang, H.; Lu, Z.; Zhou, Y.; Liang, Z.; Liu, Z.; et al. *Nano Lett.* **2014**, *14* (10), 6016−6022.
(21) Li, N. W.; Yin, Y. X.; Yang, C. P.; Guo, Y. G. *Adv. Mater.* **2016**, *28* (9), 1853−1858.
(22) Liu, K.; Pei, A.; Lee, H. R.; Kong, B.; Liu, N.; Lin, D.; Liu, Y.; Liu, C.; Hsu, P.-c.; Bao, Z.; Cui, Y. *J. Am. Chem. Soc.* **2017**, *139* (13), 4815−4820.
(23) Liang, Z.; Zheng, G.; Liu, C.; Liu, N.; Li, W.; Yan, K.; Yao, H.; Hsu, P.-C.; Chu, S.; Cui, Y. *Nano Lett.* **2015**, *15* (5), 2910−2916.
(24) Yang, C.-P.; Yin, Y.-X.; Zhang, S.-F.; Li, N.-W.; Guo, Y.-G. *Nat. Commun.* **2015**, *6*, 8058.
(25) Cheng, X. B.; Hou, T. Z.; Zhang, R.; Peng, H. J.; Zhao, C. Z.; Huang, J. Q.; Zhang, Q. *Adv. Mater.* **2016**, *28* (15), 2888−2895.
(26) Lin, D.; Zhuo, D.; Liu, Y.; Cui, Y. *J. Am. Chem. Soc.* **2016**, *138* (34), 11044−11050.
(27) Lin, D.; Liu, Y.; Liang, Z.; Lee, H.-W.; Sun, J.; Wang, H.; Yan, K.; Xie, J.; Cui, Y. *Nat. Nanotechnol.* **2016**, *11* (7), 626−632.
(28) Liu, Y.; Lin, D.; Liang, Z.; Zhao, J.; Yan, K.; Cui, Y. *Nat. Commun.* **2016**, *7*, 10992.
(29) Liang, Z.; Lin, D.; Zhao, J.; Lu, Z.; Liu, Y.; Liu, C.; Lu, Y.; Wang, H.; Yan, K.; Tao, X.; et al. *Proc. Natl. Acad. Sci. U. S. A.* **2016**, *113* (11), 2862−2867.
(30) Yan, K.; Lu, Z.; Lee, H.-W.; Xiong, F.; Hsu, P.-C.; Li, Y.; Zhao, J.; Chu, S.; Cui, Y. *Nat. Energy* **2016**, *1*, 16010.
(31) Lin, D.; Zhao, J.; Sun, J.; Yao, H.; Liu, Y.; Yan, K.; Cui, Y. *Proc. Natl. Acad. Sci. U. S. A.* **2017**, *114*, 4613.
(32) Tikekar, M. D.; Choudhury, S.; Tu, Z.; Archer, L. A. *Nat. Energy* **2016**, *1*, 16114.
(33) Zhu, Y.; He, X.; Mo, Y. *ACS Appl. Mater. Interfaces* **2015**, *7* (42), 23685−23693.
(34) Kanamura, K.; Shiraishi, S.; Takehara, Z.-i. *J. Fluorine Chem.* **1998**, *87* (2), 235−243.
(35) Shiraishi, S.; Kanamura, K.; Takehara, Z. i. *J. Electrochem. Soc.* **1999**, *146* (5), 1633−1639.
(36) Lu, Y.; Tu, Z.; Archer, L. A. *Nat. Mater.* **2014**, *13* (10), 961−969.
(37) Li, C.; Gu, L.; Maier, J. *Adv. Funct. Mater.* **2012**, *22* (6), 1145−1149.
(38) Manthiram, A.; Fu, Y.; Chung, S.-H.; Zu, C.; Su, Y.-S. *Chem. Rev.* **2014**, *114* (23), 11751−11787.
(39) Seh, Z. W.; Sun, Y.; Zhang, Q.; Cui, Y. *Chem. Soc. Rev.* **2016**, *45*, 5605−5634.

NOTE ADDED AFTER ASAP PUBLICATION

This paper published ASAP on 5/25/2017. Additional text corrections were made, and the revised version published on 5/26/2017.

DOI: 10.1021/acs.nanolett.7b01020
Nano Lett. XXXX, XXX, XXX−XXX